Copyright © 2006 Tech Science Press FDMP, vol.2, no.4, pp.271-286, 2006

Permeability and Thermodiffusion Effect in a Porous Cavity Filled with Hydrocarbon Fluid Mixtures

T. J Jaber[1], M. Khawaja[1] and M.Z. Saghir[1]

Abstract: This paper investigates numerically the interaction between thermodiffusion and buoyancy driven convection in a laterally heated vertical porous cavity for different values of the permeability. The Firoozabadi model is applied to several binary hydrocarbon mixtures: (i) a mixture of 1,2,3,4 tetrahydronaphtalene (THN) and dodecane (C12) with mass fraction of 50% for each component, (ii) 1,2,3,4 tetrahydronaphtalene and isobutylbenzene (IBB) with mass fraction of 50% for each component, and (iii) isobutylbenzene and dodecane with mass fraction of 50% for each component. The thermal and molecular diffusion coefficients, which are functions of the temperature and other properties of the mixture, are calculated at each point of the grid. Numerical results reveal that when the permeability is low the thermodiffusion effect is dominant in the composition separation process. As the permeability increases the thermodiffusion effect and buoyancy-driven convection combine their actions to enhance the composition separation process. As the permeability increases further the buoyancy-driven convection becomes dominant in the cavity and becomes detrimental to separation in the cavity.

keyword: Soret effect, Convection, Thermal diffusion coefficent, Separation ratio, Permeability, Peng-Robinson

1 Introduction

Convection in a fluid may arise from temperature differences either within the fluid or between the fluid and its boundary. The basic premise behind convection is that heated matter becomes lighter and rises, while cooler material sinks.

The thermodiffusion, also known as the Soret effect, is the tendency of a convection-free mixture to separate under a temperature gradient. For binary mixtures, the Soret effect is measured by the Soret coefficient, S_T, which is the ratio of the thermal diffusion coefficient, D^T, to the molecular diffusion coefficient D^M. However, for multicomponent mixtures, the thermal diffusion coefficient is more commonly used as a measure of the Soret effect. The Soret effect is an important phenomenon for the study of the compositional variation in hydrocarbon reservoirs. It also plays a crucial role in the hydrodynamic instability of mixtures, mineral migrations and mass transport in living matters.

Convection has a major influence on the accuracy of the Soret measurements. Utilization of porous media helps in reducing the distortion caused by convection because the fluid moves slowly in porous media. Costeseque *et al.* (2004) conducted experiments in both a free fluid and a porous medium with a vertical temperature gradient. It was found that, when the thermal conductivities of the fluid and solid matrix are of the same magnitude, the Soret coefficients do not differ significantly with respect to the case of the free fluid.

Several researchers have published values of the Soret coefficient for organic molecules, polymers, and even electrolytes solutions. In particular, in 1999, research groups from different universities started a ground-based measurement campaign (see Platten et al (2003)). The goal was to establish a reliable database of the Soret coefficient for three binary mixtures composed of dodecane (C12), Isobutylbenzene (IBB), and 1,2,3,4-tetrahydrophtalene (THN). As well, there was a clear desire to establish benchmark values for the Soret, thermal diffusion, and diffusion (Fick) coefficients so that they could be used to compare Earth results with results obtained through other means such as experiments in microgravity or numerical simulation. The values obtained from independent researchers, were in strong agreement with each other, Platten *et al.* (2003), their differences did not exceed 7%.

Despite the fact that transport coefficient data for binary mixtures is available, it is known, however, that the vari-

---

[1] Ryerson University, Department of Mechanical and Industrial Engineering, 350 Victoria Street, Toronto, ON. M5B 2K3 Canada

ation of hydrocarbon reservoirs for a non-ideal multicomponent mixture system cannot be determined using results obtained from binary mixtures since diffusion coefficients may significantly differ in multi-component mixtures. Shukla and Firoozabadi (1998) developed a model for thermal diffusion factors in multi-component non-ideal mixtures. This model was based on the thermodynamics of irreversible processes where the effects of both equilibrium and non-equilibrium properties are incorporated. The equilibrium properties, such as partial internal energies and fugacities, were estimated using the volume-translated Peng-Robinson equation of state. On the other hand, the non-equilibrium properties, such as viscosity, were accounted for by incorporating the energy of viscous flow. The model was validated with the measured compositional data for a ternary mixture $nC_{21}/nC_{16}/nC_{12}$. They further predicted the thermodiffusion behaviour for a six-component mixture of $C_1/C_3/nC_5/nC_{10}/nC_{16}/C_2$ at various temperatures and pressures and found that when the system was far from the critical point, the thermal diffusion factor was not sensitive to temperature or pressure.

Firoozabadi *et al.* (2000) further examined the performance of this model for three different binary systems; the hydrocarbon system, i.e. C_1/C_3, C_1/C_4, C_7/C_{12} and C_7/C_{16}, the non-hydrocarbon system, i.e. Ar/CO_2, N_2/CO_2, H_2/N_2, and H_2/CO_2, and the hydrocarbon-nonhydrocarbon system, i.e. C_1/N_2 and C_1/CO_2. These three systems were used to model binary mixtures of reservoir fluids. The model was compared with experimental data and two other models: the Rutherford and Kempers models, see Kempers (1989) and Rutherford *et al.* (1959). It is worth noting that when detailed comparison is made between the theoretical results and the experimental data, the Firoozabadi model is superior in describing experimental results for the thermal diffusion coefficients in binary mixtures. In particular, the sign of thermal diffusion coefficient is consistent with the experimental data.

A study by Lorenz and Emery (1959) showed that the maximum magnitude of separation or the optimum coupling between buoyancy and thermodiffusion is obtained at a particular value of the permeability. Benano-Melly *et al.* (2001) numerically investigated the phenomenon of thermo gravitation convection in binary fluid mixtures. In their study, a two-dimensional cell with two vertical walls set at constant different temperatures was used. The binary mixture filling the cell porous medium was initially homogenous, and the two-dimensional cell's boundary condition was no flow and no mass flux through the cell walls. The flow analysis showed that the mixture undergoes convection due to the presence of thermal gradient with higher convection velocity near the cell vertical sides. It was found that when the solutal Rayleigh number is high enough, and the Soret number is positive, the solutal and thermal buoyancy forces combine their actions to enhance convection, and when the Rayleigh number is high and the Soret number is negative, the counteracting solutal and thermal buoyancy forces weaken the convection. It was also observed that the solutal buoyancy force had negligible, or no effect, on the convection for solutal Rayleigh numbers lower than 0.1. Benano-Melly *et al.* (2001) further investigated the solute migration and distribution behavior and found that the amplitude of the separation ratio mainly depends on the thermal Rayleigh number; also, a decreased Lewis number results in a decreasing separation ratio.

Riley and Firoozabadi (1998) presented a model to investigate the effects of natural convection and diffusion (thermal, pressure and fickian) on a single-phase binary mixture Methane-nButane in a horizontal cross-sectional reservoir in the presence of a prescribed linear temperature field. It was found that increasing the permeability increases the horizontal compositional variation. A local maximum and/or minimum value exists in the compositional gradient as a function of the permeability.

The objective of this study is to numerically investigate the interaction between thermodiffusion and buoyancy driven convection in a laterally heated vertical porous cavity with an aspect ratio of 10 filled with three binary mixtures of THN-C12, IBB-C12, and THN-IBB. The thermodiffusion process is simulated in a vertical porous cavity with permeability ranging from 0.001 md to 10,000 md. Section two introduces the numerical model, section three presents mathematical modelling. The solution technique is explained in section four and the results and discussions are shown in section 5.

2 The Numerical model

A vertical cavity with height (H) of 5 m and width (W) of 0.5 m is considered with various boundary conditions, as shown in Figure 1. The four walls are assumed to be non-reacting, solid, impermeable, and with no-slip condition.

Two lateral walls have a Dirichlet boundary condition; the right wall with hot temperature of 303 K, and the left wall with cold temperature of 293 K. The top and bottom walls are assumed to be adiabatic. The binary mixtures filling the vertical cavity consist of THN-C12, IBB-C12, and THN-C12, each component at 50% mass fraction, and under atmospheric pressure. The fluid is considered to be compressible, with no heat generation, no chemical reaction, and no interactive superficial forces acting between the porous medium particles and the liquid mixture.

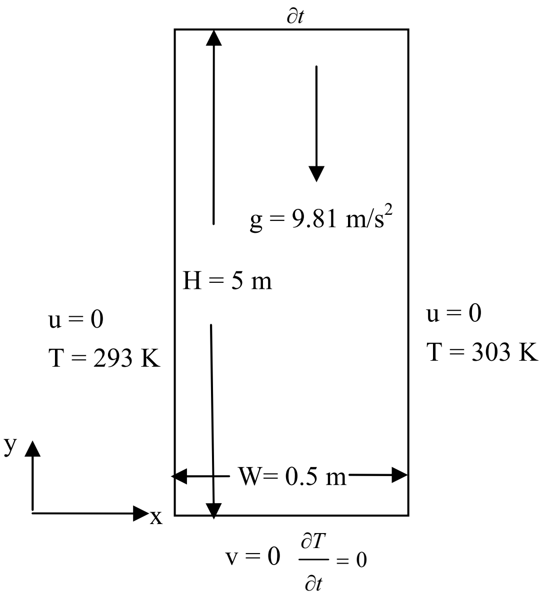

Figure 1 : Two-dimensional porous media model and boundary conditions

3 Mathematical Modelling

In order to simulate the thermodiffusion process in a porous medium cavity, field equations describing the response of the mixture fluid to thermo-solutal and gravitational driving forces are required. Therefore, a mass continuity equation, a momentum conservation equation and an energy conservation equation are introduced.

3.1 Mass Continuity Equation

In a two-dimensional domain, the general conversation of mass equation can be written in the following form:

$$\frac{\partial \rho_m}{\partial t} + \frac{\partial(\rho_m u)}{\partial x} + \frac{\partial(\rho_m v)}{\partial y} = 0 \tag{1}$$

where: ρ_m is the molar density of the mixture fluid, and u and v are the horizontal and vertical velocity components, respectively. Since a multicomponent mixture is used, an additional mass conversation equation is solved, namely:

$$\frac{\partial(\rho_m c)}{\partial t} + \frac{\partial(\rho_m uc)}{\partial x} + \frac{\partial(\rho_m vc)}{\partial y} = -\nabla \bullet \overline{J} \tag{2}$$

where: $\overline{J}$ is the molar flux of the solute and can be written in general form as follows:

$$\vec{J} = -\rho_m \left(D^M \nabla c + D^T \nabla T + D^P \nabla P\right) \tag{3}$$

where: D^M is the molecular diffusion coefficient; D^T is the thermal diffusion coefficient; D^P is the pressure diffusion coefficient; ∇c is the mole fraction gradient; ∇P is the pressure gradient; ∇T is the temperature gradient.

3.2 Momentum Conservation Equation

In porous media, the porous matrix is assumed to be homogenous and isotropic, therefore, the Darcy's equation can be applied and expressed in the following form:

$$\vec{V} = -\frac{\kappa}{\phi \mu}\left(\nabla P - \rho \vec{g}\right) \tag{4}$$

where: ρ is the mass density of the fluid mixture, κ is the permeability, ϕ is the porosity, μ is the dynamic viscosity, and $\vec{g}$ is the gravity acceleration vector. $\vec{V} = u\vec{i} + v\vec{j}$ is the velocity vector in the two dimensional field. By substituting the Darcy's equation into the general conservation of mass equation (1), a pressure differential equation is obtained:

$$\frac{\partial(\rho_m)}{\partial t} - \frac{\kappa}{\phi \mu}\frac{\partial}{\partial x}\left(\rho_m \frac{\partial P}{\partial x}\right) - \frac{\kappa}{\phi \mu}\frac{\partial}{\partial y}\left(\rho_m\left(\frac{\partial P}{\partial y} + \rho g\right)\right) = 0 \tag{5}$$

3.3 Energy Conservation Equation

The energy conservation equation can be expressed as follows for a two-dimensional domain and with Darcy's equation substituted in it:

$$\frac{\partial(\rho C_p)_e T}{\partial t}+\phi u\frac{\partial}{\partial x}\left((\rho C_p)_f T\right)+\phi v\frac{\partial}{\partial y}\left((\rho C_p)_f T\right) = k_e\left[\frac{\partial^2 T}{\partial x^2}+\frac{\partial^2 T}{\partial y^2}\right] \quad (6)$$

where: $(\rho C_p)_e$ is the effective volumetric heat capacity of the system and k_e is the effective thermal conductivity of the system. These effective physical parameters are related to the fluid properties and the solid matrix properties as $(\rho C_p)_e=\phi\,(\rho C_p)_f+(1-\phi)\,(\rho C_p)_p$ and $k_e=\phi k_f+(1-\phi)k_p$.

4 Numerical Solution Technique

Equations (1), (2), (5), and (6) together with their corresponding boundary conditions as depicted in Figure 1, are numerically solved using a control volume method with a rectangular grid system. The second-order centered scheme is used in the space discretization, and a semi-implicit first-order scheme is used for the temporal integration. With respect to the non-linear convection terms, power-law scheme [Rutherford *et al.* (1959)] is applied in order to achieve higher accuracy for the combined convection and diffusion cases. The obtained linear system of algebraic equations is solved at each time step using a bi-conjugated gradient iteration method with a given convergence criterion, which has been confirmed over many tests for the required accuracy. At the initial time step, the velocities were set to zero in the computational domain where initial pressure and concentration are specified. The convergence criterion is set for three parameters, the pressure P, temperature T and concentration c, respectively. The errors between iterations are calculated as follows:

$$\gamma_\theta=\frac{1}{m\times n}\sum_{i=1}^{m}\sum_{j=1}^{n}\left|\frac{\theta_{ij}^{k,s+1}-\theta_{ij}^{k,s}}{\theta_{ij}^{k,s+1}}\right| \quad (7)$$

where: θ represents the pressure, temperature or concentration, i and j represent mesh indices along x and y directions of the domain; k denotes the time step, and s is the indicator of inner iterations. The values of pressure, temperature and concentration are defined at the center of each control volume, but the velocities are defined on the surface of each control volume, or grid cell. Different mesh sizes were tested and a 71 x 71 control volume was adopted. The solution procedure begins by assuming initial pressure, temperature and concentration values in the mixture. Since the Peng-Robinson Equating (EOS), Firoozabadi (1999), is used to calculate the density variation, as well as other fluid properties, the flow is considered to be compressible. Therefore, the properties of the liquid, such as the density, viscosity, specific heat and all three diffusion coefficients are functions of the temperature, pressure and the fluid mixture composition and are evaluated for each control volume. The thermal conductivity is assumed constant in the analysis.

In this paper, the viscosity of the liquid mixture (μ) is obtained with a method proposed by Lohrenz et al. (1964) and given by:

$$\mu=\mu^*+(\xi^4-10^{-4})/\xi \quad (8)$$

where μ^* is the gas-mixture viscosity (Jossi et al 1961), ζ is the mixture viscosity parameter and ξ is a variable related to the reduced density (ρ_r) with a fourth order polynomial.

The calculation of the three diffusion coefficients is well explained in the papers by Firoozabadi *et al.* (2000), Shukla and Firoozabadi (1998) and Chacha *et al.* (2003). Once the properties of the liquid and all three diffusion coefficients are obtained, the continuity equations (1) and (2), velocity equation (4), pressure equation (5) and the energy equation (6) can be solved with the given boundary conditions. The updated pressure, temperature, and concentration fields can be used to evaluate the liquid properties and all three diffusion coefficients again for the next time step until steady state is achieved.

Finally, the stream function is computed via solution of the related well-known Poisson equation.

$$\frac{\partial^2\Psi}{\partial x^2}+\frac{\partial^2\Psi}{\partial y^2}=\frac{\partial u}{\partial y}-\frac{\partial v}{\partial x} \quad (9)$$

5 Results and discussion

In order to make the analyses more realistic, wide ranges of permeabilities are utilized. The permeability ranges from 0.001 md to 10,000 md, corresponding to a Darcy number of 3.91 x 10^{-20} to 3.91 x 10^{-13} respectively and the porosity is set equal to 0.2. The numerical simulation is used to analyze the flow characteristics, the velocity in the cavity, the component migration, and concentration gradients. The separation ratio is also calculated and compared with analytical values.

5.1 Comparison of flow patterns

The streamlines indicating the flow behaviours for THN-C12, IBB-C12, and THN-IBB are depicted in Figures 2, 4, and 6, respectively.

The streamlines show that for all three binary mixtures and k=0.001 md (low permeability) the flow is very weak. This is also evident in Figures 3, 5, and 7, which show the vertical velocities along the center of the cavity for the three binary mixtures. As the permeability increases, the flow gains strength in all three binary mixtures. As shown in Figures 3, 5 and 7, when the permeability increases the fluid flow becomes stronger and causes the fluid to go up along the hot wall, and then down along the cold wall, creating a counter-clockwise flow in the cavity.

The flow behaviour in all three mixtures can be explained by realizing that at low permeability the porous medium is tightly packed. The porous media has a texture that makes it difficult for the fluid mixture to flow, hence, controlling or reducing the convection. The lateral heat applied to the cavity containing the porous media creates a temperature gradient inside the cavity, which causes thermodiffusion to occur. The thermodiffusion or the Soret effect is therefore dominant in the cavity at low permeabilities. As the permeability increases the porous media becomes more pervious. It assumes a texture similar to very fine sand. At even higher permeability the porous media becomes almost like well sorted gravel. Therefore, the porous media allows the mixtures to flow, contributing to the higher fluid velocities in the cavity. In such conditions, the buoyancy-driven convection becomes dominant in the cavity, which in turn has a negative effect on the thermodiffusion. At high permeability values, the convection completely overwhelms the thermodiffusion. One of the differences noticed between the three binary mixtures is that the highest velocity among the three mixtures occurs in the THN-C12 mixture, while the lowest velocity occurs in the THN-IBB mixture.

5.2 Comparison of density distribution along the center of the cavity vertically and horizontally

The density distribution can be regarded as a good indicator of the uniformity or separation of the mixture inside a cavity, and the way components of a mixture react to various conditions.

Figure 8 shows the density variation horizontally along the center of the cavity for the THN-C12 mixture. For low permeability, the density decreases linearly along the width of the cavity. This linear variation also suggests that the Soret effect is dominant and causes separation in the mixture, which confirms the trend seen in the flow pattern. The heavier component, THN, migrates to the cold wall, while the lighter component, C12, migrates to the hot wall. As the permeability increases the density variation remains almost linear, however, a slight curve appears in the variation. This is due to the increase in the counter-clockwise flow of the fluid mixture caused by the buoyancy-driven convection. As the permeability increases further, the buoyancy-driven convection becomes stronger, and the curve in the variation becomes more apparent. The curvature in the variation indicates that the density gradient in the cavity is diminishing, suggesting that mixing is taking place. The average density for THN-C12 mixture was found to be approximately 803 kg/m^3.

Figure 9 displays the graph with density variation vertically along the center of the cavity for the aforementioned THN-C12 mixture. At lower permeability, a uniform density distribution is observed. At such low permeability, the flow is very weak, and the linear horizontal temperature distribution causes a separation in the horizontal direction. As the permeability increases, the vertical density distribution varies linearly. This change comes from the buoyancy-driven convection, which is becoming dominant in the cavity. The heavier component, THN, is being pushed downwards by convection to the bottom of the cavity. Conversely, the lighter component, C12, is being pushed upwards to the top of the cavity. As the permeability increases further the variation becomes almost uniform again with noticeable changes near the top and bottom of the cavity. In practice, as explained before, the buoyancy-driven convection at higher permeabilities causes the flow to increase in speed. Therefore, as the fluid moves rapidly along the top and bottom boundaries of the cavity the variation becomes noticeable, while mixing takes place along the rest

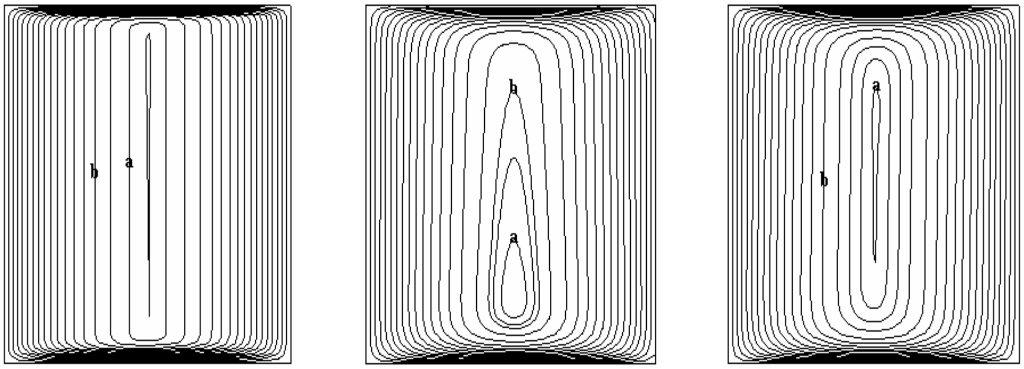

a) k= 0.001 md
$a = 3.007 \times 10^{-11}$
$b = 2.669 \times 10^{-11}$
$\Delta\psi = 3.380 \times 10^{-12}$

b) k= 10 md
$a = 3.029 \times 10^{-7}$
$b = 2.945 \times 10^{-7}$
$\Delta\psi = 8.440 \times 10^{-8}$

c) k=10,000 md
$a = 3.758 \times 10^{-4}$
$b = 1.538 \times 10^{-4}$
$\Delta\psi = 2.220 \times 10^{-5}$

Figure 2 : Streamline contours for THN-C12

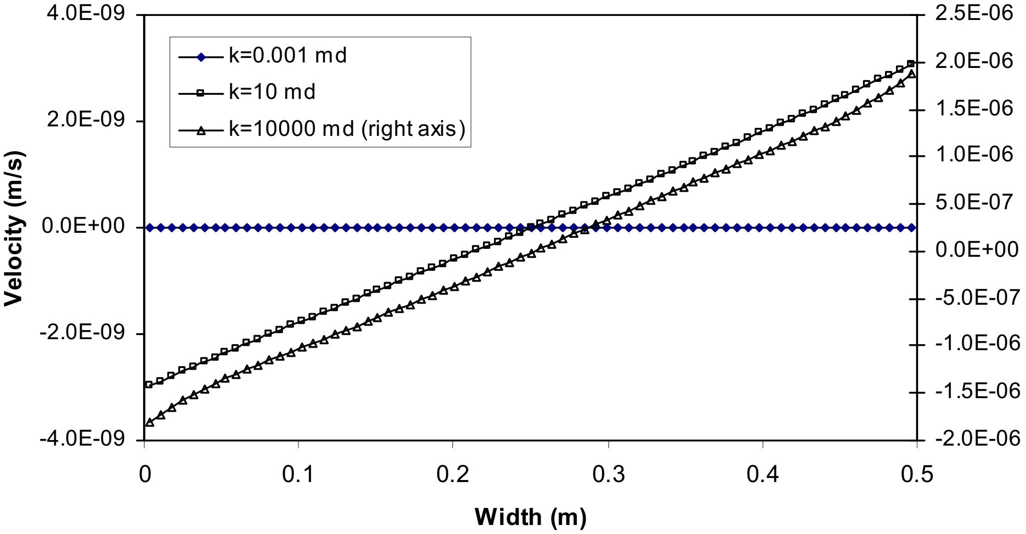

Figure 3 : Vertical velocity along the center of the cavity for THN-C12

of the cavity thereby creating uniformity in the domain.

Figure 10 presents the density variation for IBB-C12 mixture horizontally along the center of the cavity. It shows a pattern similar to the THN-C12 mixture horizontal density variation. It is evident that the density varies linearly at low permeability due to the Soret effect, while the density variation becomes non-linear as the permeabilities increase due to buoyancy convection. The only difference between the two cases is the fact that when the permeability increases, the curvature in the density variation is not as pronounced, as was the case for THN-C12 mixture. This is due to the fact that IBB is much more viscous then THN. The average density of IBB-C12 mixture is approximately 800 kg/m^3.

Figure 11 shows the density variation for IBB-C12 vertically along the center of the cavity. Once again, at lower permeability a uniform density variation is observed, and the variation becomes linear with the increase in the permeability. The change from uniform to linear variation is the result of the convection gaining strength, and causing the IBB to migrate to the bottom of the cavity. As the permeability increases further, the mixture becomes uniform throughout most of the cavity; however, there exists a sharp variation in the density near the top and bottom of the cavity as noticed earlier in the case of THN-C12 mixture.

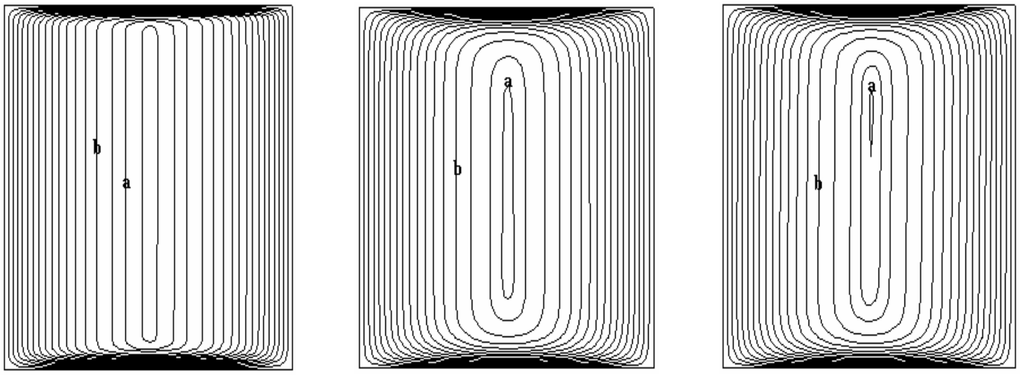

a) k= 0.001 md
$a = 1.954 \times 10^{-11}$
$b = 1.769 \times 10^{-11}$
$\Delta\psi = 1.176 \times 10^{-12}$

b) k= 10 md
$a = 2.113 \times 10^{-7}$
$b = 1.853 \times 10^{-7}$
$\Delta\psi = 1.238 \times 10^{-8}$

c) k=10,000 md
$a = 1.484 \times 10^{-4}$
$b = 1.206 \times 10^{-4}$
$\Delta\psi = 8.698 \times 10^{-6}$

Figure 4 : Streamline contours for IBB-C12

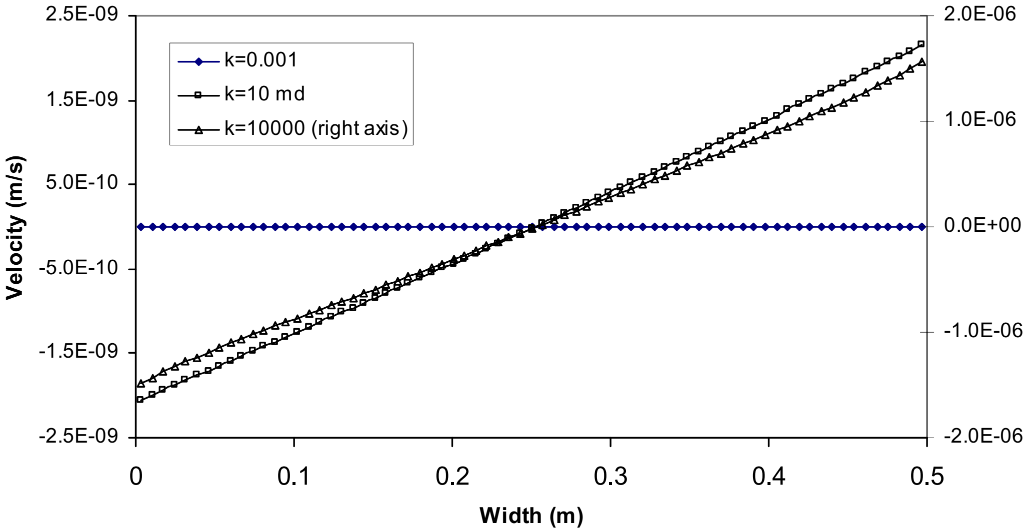

Figure 5 : Vertical velocity along the center of the cavity for IBB-C12

Figure 12 shows the density variation of the THN-IBB mixture horizontally along the center of the cavity. Contrary to the other binary mixtures of THN-C12 and IBB-C12, the THN-IBB mixture varies linearly for all ranges of permeabilities. There is little curvature in the density variation as the permeability increases, because the mixture is very viscous. Even at higher permeabilities, where convection is dominant, it is difficult to move the mixture enough to cause mixing, as was the case for the other binary mixtures. The vertical density variation along the center of the cavity is examined in Figure 13. It is evident that variation is modest compared to the other binary mixtures. The vertical density variations along the center of cavity have a tendency to remain uniform. The average density of THN-IBB mixture is approximately 903.14 kg/m^3.

5.3 *Variation of Concentration with permeability*

In Figure 14 it is evident that when the permeability is low (less than 0.1 md), a horizontal composition gradient appears because of the Soret effect. The heavier component THN migrates to the cold wall, which agrees with the previous discussions when density variation was examined. As the permeability increases, the concentration gradient direction changes, and as the permeability in-

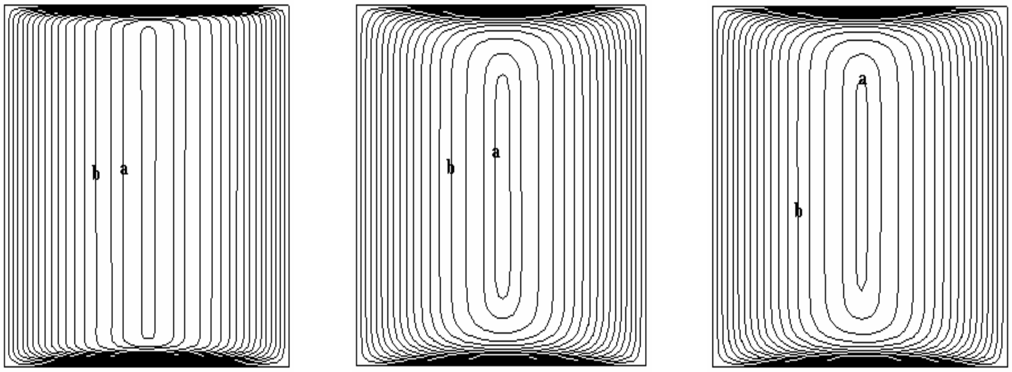

a) k= 0.001 md
a = 1.398 x 10^{-11}
b = 1.315 x 10^{-11}
$\Delta\psi$ = 8.194 x 10^{-13}

b) k= 10 md
a = 1.506 x 10^{-7}
b = 1.227 x 10^{-7}
$\Delta\psi$ = 8.819 x 10^{-9}

c) k=10,000 md
a = 1.503 x 10^{-4}
b = 1.222 x 10^{-4}
$\Delta\psi$ = 8.802 x 10^{-6}

Figure 6 : Streamline contours for THN-IBB

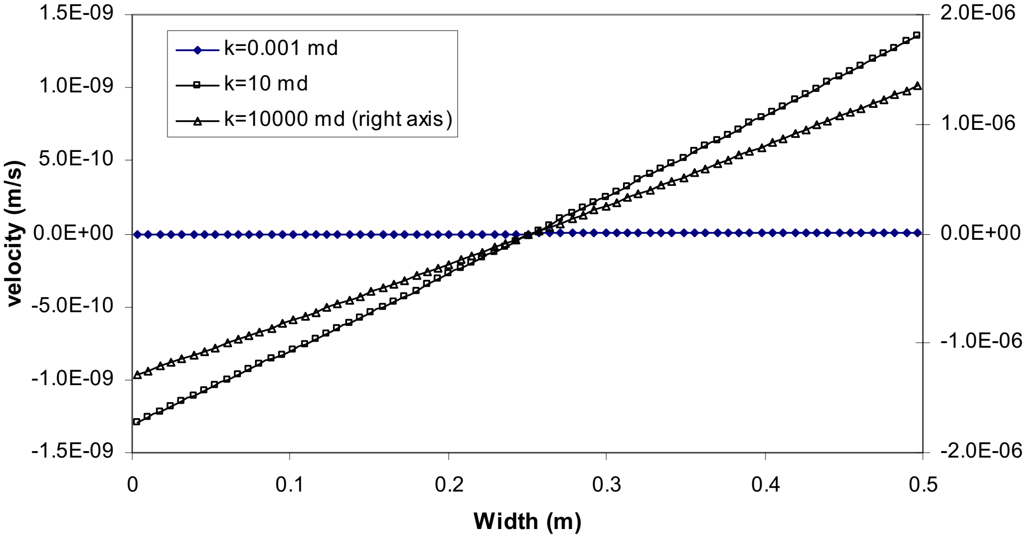

Figure 7 : Vertical velocity along the center of the cavity for THN-IBB

creases further it assumes an angle of almost 45 degrees (k=10 md). The change in direction again points to the fact that the buoyancy-driven convection is increasing in strength, and causing the fluid to flow inside the cavity. As the permeability continues to increase, the concentration gradient becomes almost vertical (k=100 md) with heavier THN accumulating near the bottom of the cavity, which once again agrees with the earlier findings. At high permeability values, the concentration gradient no longer exists, and a clear mixing pattern is visible, with flow moving in a counter-clockwise direction. A similar pattern is seen in the binary mixture of IBB-C12, Figure 15, and THN-IBB, Figure 16. The concentration gradient is horizontal at low permeability, then it changes direction to almost 45 degrees as permeability increases. The gradient is caused by the contribution of both the Soret effect and the buoyancy-driven convection. As the permeability increases, the buoyancy-driven convection becomes dominant. This will lead to a uniform concentration in the cavity as shown in Figure15c and Figure 16c.

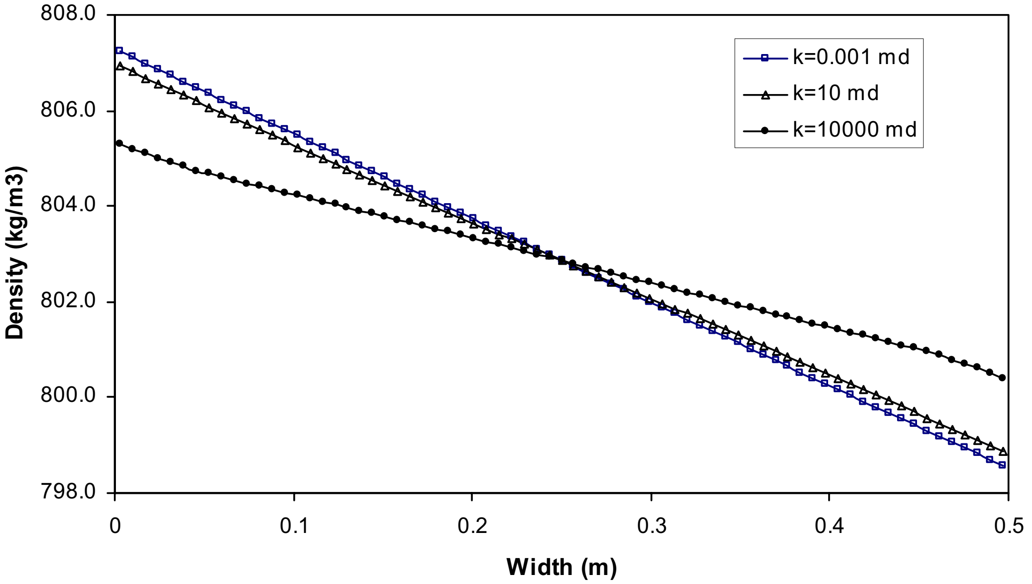

Figure 8 : Horizontal density distribution for THN-C12

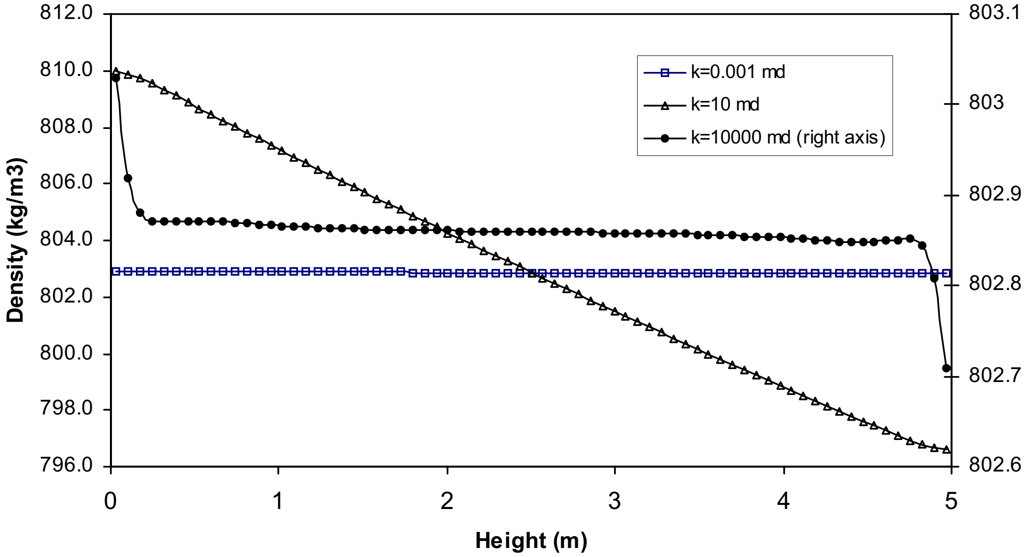

Figure 9 : Vertical density distribution for THN-C12

5.4 *Separation Ratio*

It is evident that the permeability has a direct effect on the separation of the components in the mixture. At lower permeability the Soret effect has a significant impact on the mixture, while at higher permeability convection becomes a major factor. One method of further examining the effect of permeability can be based on the introduction of a variable known as the separation ratio (q). The separation ratio can be defined as follows:

$$q = \frac{C_{\max}/(1-C_{\max})}{C_{\min}/(1-C_{\min})} \tag{10}$$

where: C_{max} represents the maximum concentration and C_{min} represents the minimum concentration of a solute component in the whole porous cavity.

A variation in the separation ratio as a function of the permeability is shown in Figure 17. The separation ra-

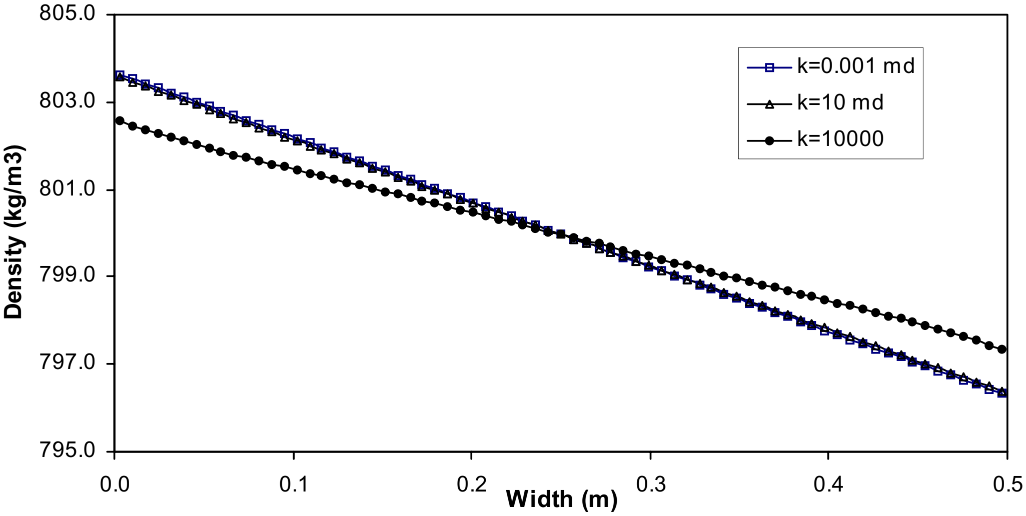

Figure 10 : Horizontal density distribution for IBB-C12

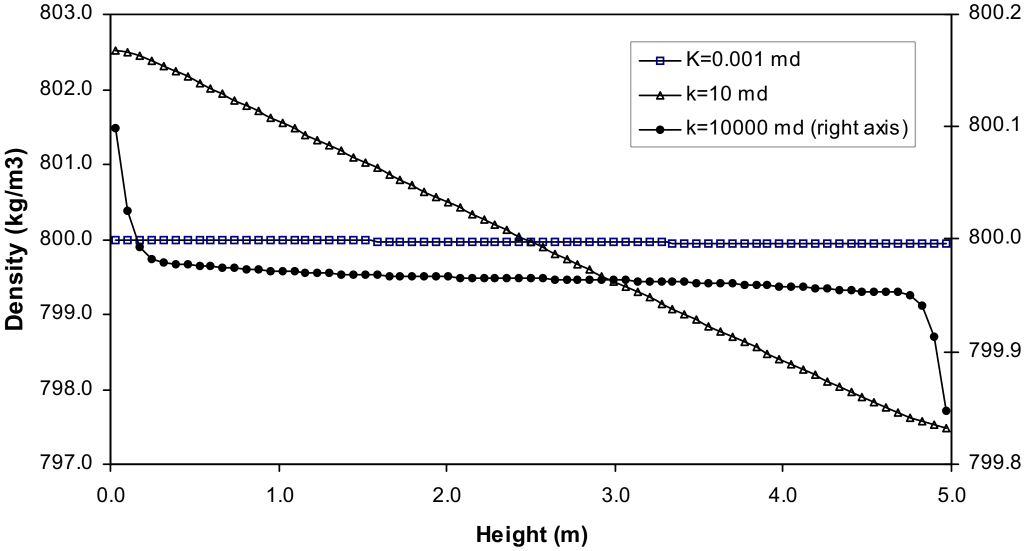

Figure 11 : Vertical density distribution for IBB-C12

tio variation along with permeability indicates three noticeable regions. The first region is between 0.001 and 0.1 md, where the separation ratio remains constant and maintains a value above 1. This region is caused by the strong thermodiffusion, while the convection effect is negligible. Therefore, a value of separation ratio that is close to the value of one (q=1) specifies that the Soret effect is weak, and a value far from the value of one (q=1) indicates that the Soret effect is stronger and causing perceptible separation in the cavity. Among the three binary mixtures, the Soret effect is strongest at lower permeability in the THN-C12 mixture, while it is weakest in the THN-IBB case.

The second region is between 0.1 and 1000 md. In this region, the separation ratio value increases and reaches a peak value. This peak value indicates the permeability value where the maximum separation of components occurs. The increase in the Separation ratio also indicates the change in orientation in the concentration gradient. The concentration gradient, when increasing the permeability, slowly becomes horizontal. The maximum separation occurs when the heavier component accumulates on the bottom of the cavity near the cold wall, and the lighter component accumulates on the top of the cavity

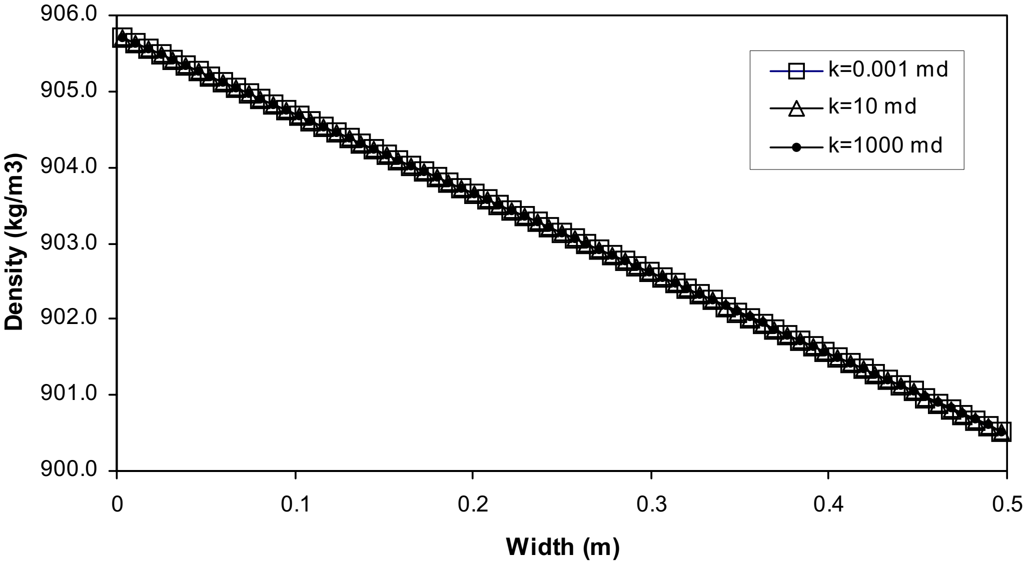

Figure 12 : Horizontal density distribution for THN-IBB

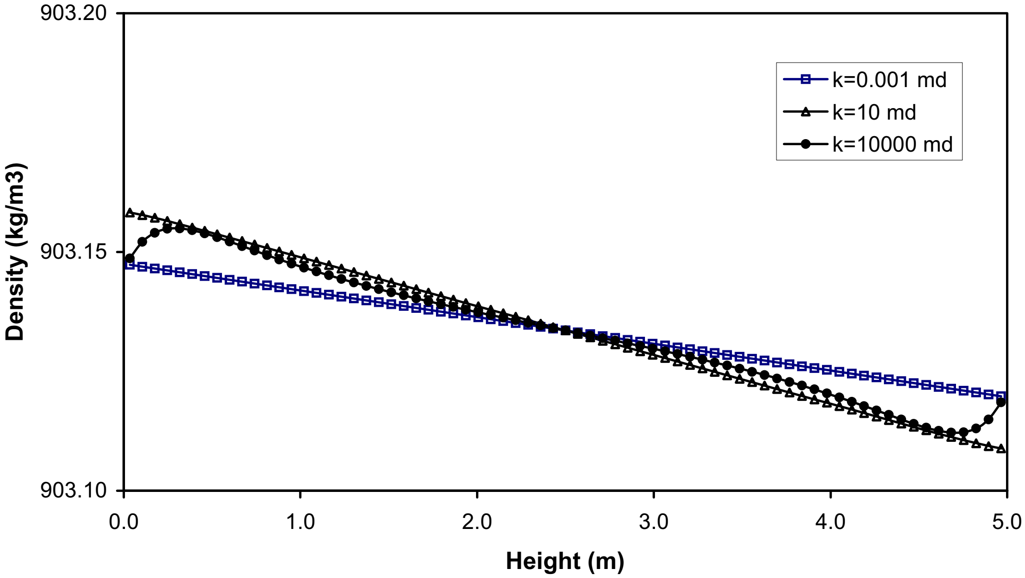

Figure 13 : Vertical density distribution for THN-IBB

near the hot wall. This region also indicates that separation is caused by the contribution of both the Soret effect and the buoyancy-driven convection. It is found that the THN-C12 mixture has the highest value of Separation ratio, while the THN-IBB mixture has the lowest value.

The third region is between 1000 md and 10,000 md. In this region, the separation ratio decreases rapidly and reaches a value close to 1, (because the buoyancy-driven convection causes the mixture to mix). In this region, the convection becomes dominant and the Soret effect is suppressed.

Benano-Melly *et al.* (2001) showed that a maximum value for the separation ratio exists for a permeability given by the following expression:

$$\kappa = \frac{\mu D^M \phi \sqrt{120}}{g \beta_T \Delta T H \rho} \tag{11}$$

Table 1 shows the maximum separation according to the analytical expression and the value of maximum separation obtained by the present numerical simulation. The

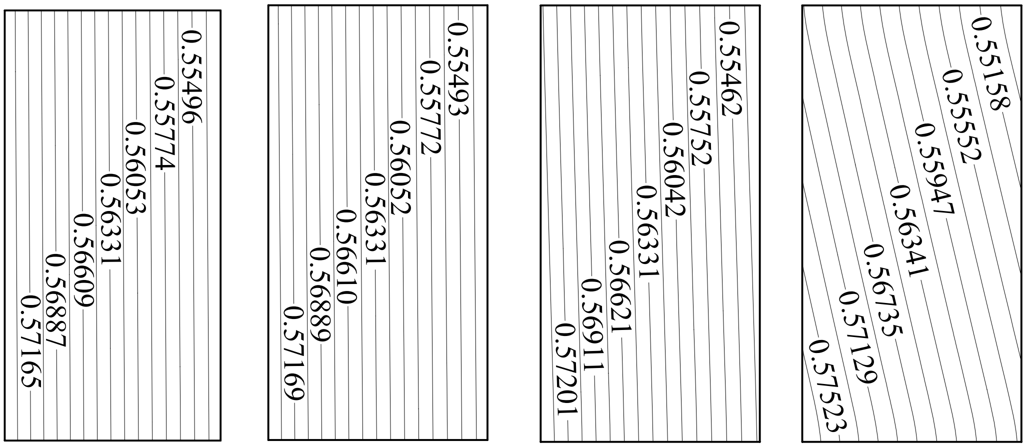

(a) k = 0.001 md (b) k = 0.01 md (c) k = 0.1md (d) k = 1 md

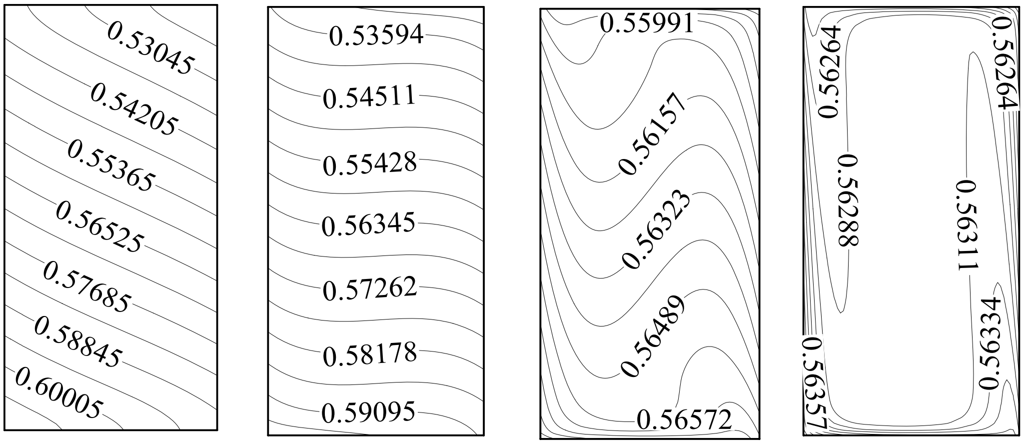

(e) k = 10 md (f) k = 100 md (g) k = 1000 md (h) k = 10000 md

Figure 14 : Concentration contours for permeability range from 0.001 md to 10000 md for THN-C12

discrepancy between the values obtained by analytical expression and by numerical modeling is due to the fact that solutal buoyancy is included in the numerical simulation. In addition, in the present simulations, both thermal and molecular diffusion coefficients are functions of temperature, fluid mixtures, and pressure.

Peaking of the separation ratio in the second region might be explained according to the fluid and thermal characteristic times shown in Figure 18 for the THN-C12. The characteristic time for thermodiffusion τ_{th} (i.e. Tau_th in the graph) is found to be constant at 1.17 x 10^8 seconds, while the flow characteristic time τ_f (i.e. Tau_f in the graph) decreases monotonically from 1 x 10^{10} seconds to 3.69 x 10^6 seconds, as the permeability increases. The point of intersection of the fluid characteristic time and the thermal characteristic time occurs at approximately 25 md, which corresponds to the value of permeability where the separation ratio is observed to be at its maximum value. Consequently, the point of intersection also indicates that beyond this point the fluid characteristic time will be less than the thermal characteristic time, hence, indicating that the buoyancy-driven convection becomes the dominant force in the cavity.

Another way to study this effect is by plotting the ratio of solutal Rayleigh number (Ra_c) and thermal Rayleigh number (Ra_T) as a function of the permeability as shown in Figure 19. The ratio can be defined as follows:

$$\frac{Ra_c}{Ra_T} = Le\frac{\beta_c \Delta c}{\beta_T \Delta T} \tag{12}$$

where Le is the Lewis number. The Rayleigh number is defined as the product of the Grashof number, which

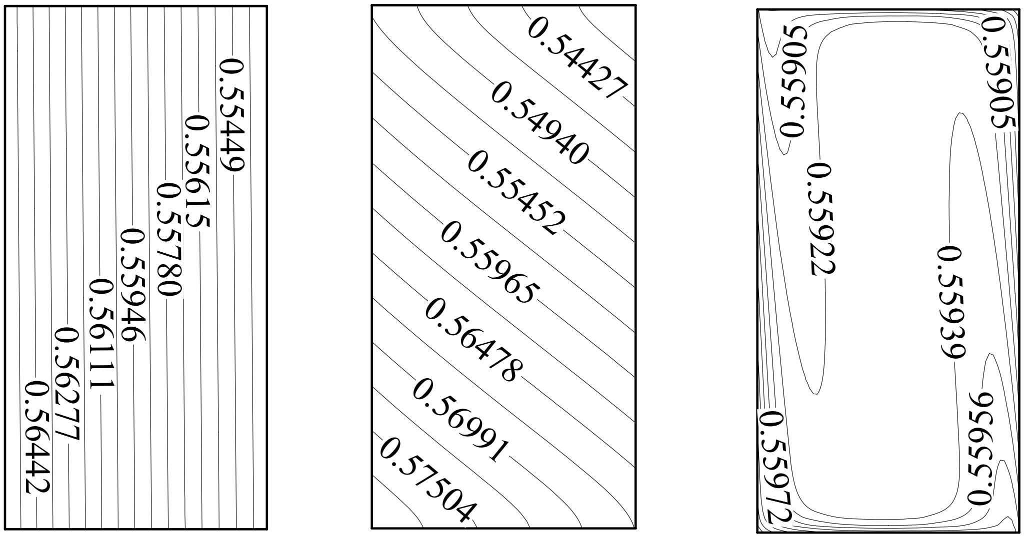

(a) k = 0.001 md (b) k = 10 md (c) k = 10000 md

Figure 15 : Concentration contours for IBB-C12

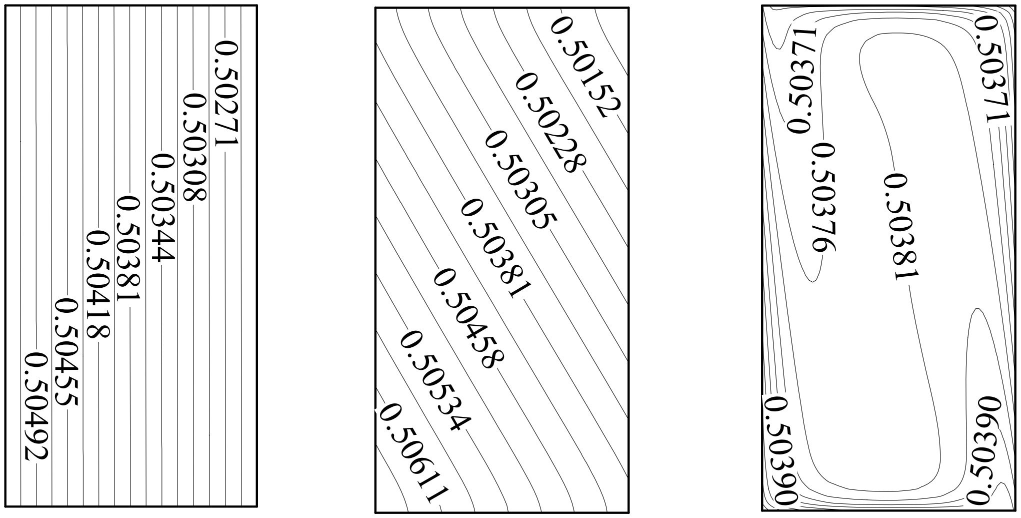

a) k = 0.001 md (b) k = 10 md (c) k = 10000 md

Figure 16 : Concentration contours for THN-IBB

describes the relationship between buoyancy and inertia within a fluid, and the Prandtl number. Figure 19 illustrates that the concentration difference remains uniform for permeability between 0.001 and 0.1 md, because the ratio of Rayleigh numbers remains constant. The concentration difference increases from 0.1 md to 10 md, and then decreases from 10 md to 10,000 md. It can be realized that for permeability between 0.1 md and 10 md, as the thermal Rayleigh number increases linearly, the solutal Rayleigh number begins to increase linearly as well, indicating the dominance of the Soret effect. Between 10 md and 100 md, there is a slight increase and then a peak occurs around 25 md indicating that the Soret effect and buoyancy-driven convection are both active in the cavity. Above a permeability of 25 md, there is a reduction in the solutal Rayleigh number; however, the thermal Rayleigh number continues to increase linearly indicating the dominance of buoyancy-driven convection.

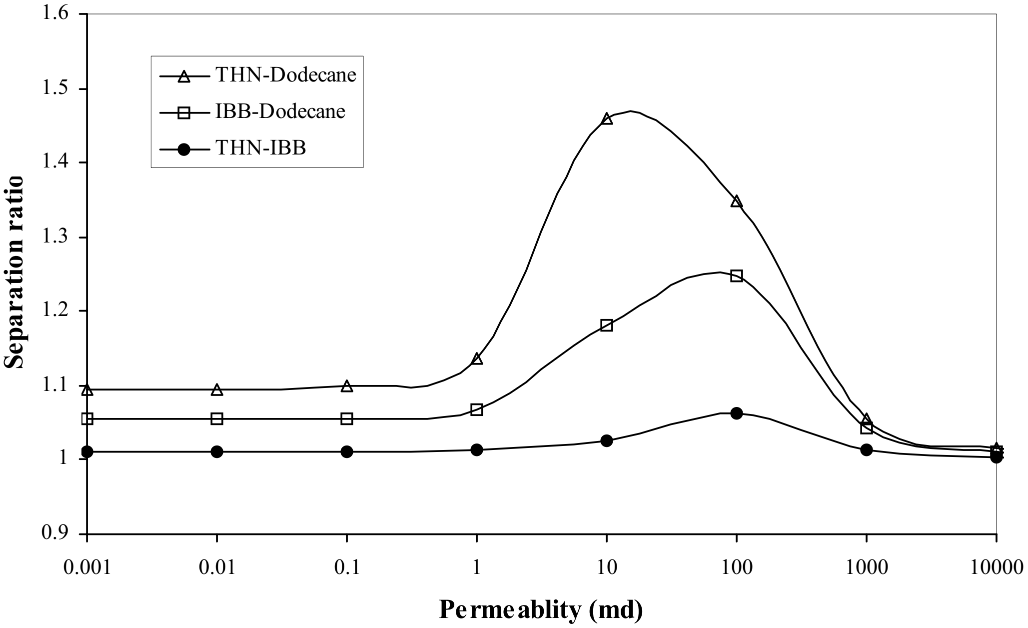

Figure 17 : Separation ratio as a function of the permeability

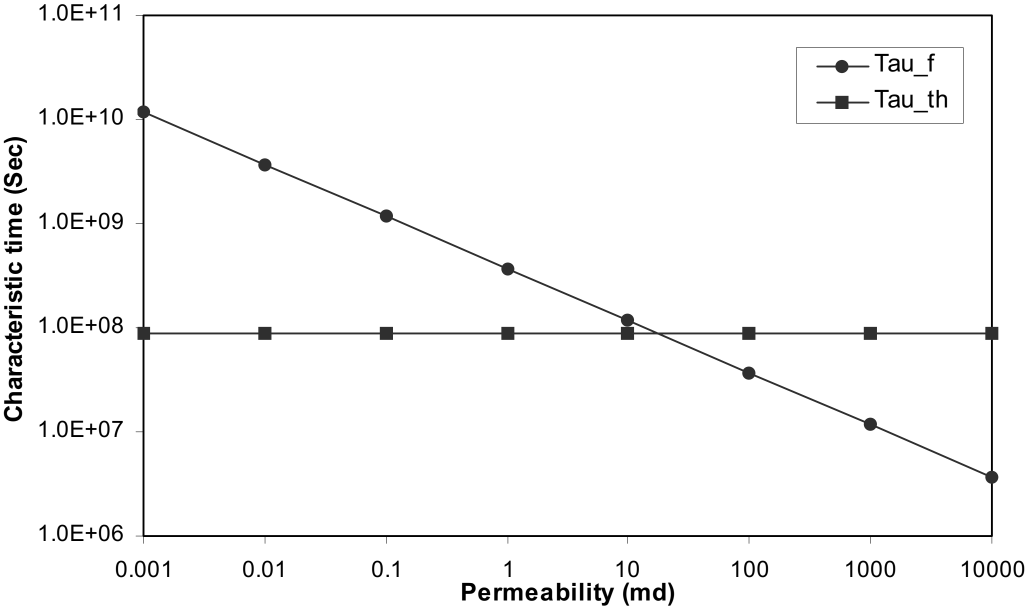

Figure 18 : Characteristic times as a function of the permeability

6 Conclusion

This study has investigated the interaction between thermodiffusion and buoyancy driven convection in a single-phase hydrocarbon binary mixture system. Three binary mixtures of THN-C12, IBB-C12, and THN-IBB, each with 50% mass fraction, were used in the simulation.

The model was based on the non-equilibrium thermodynamics theory and the diffusion coefficients were evaluated with time and space dependent fluid properties and compositions. In the analysis, the flow characteristics, the velocity in the cavity, the component concentration gradients, and the separation ratio were used to investigate the behaviour of the thermodiffusion and buoyancy-driven convection. It has been found from the density pattern that at low permeability the lateral heating pro-

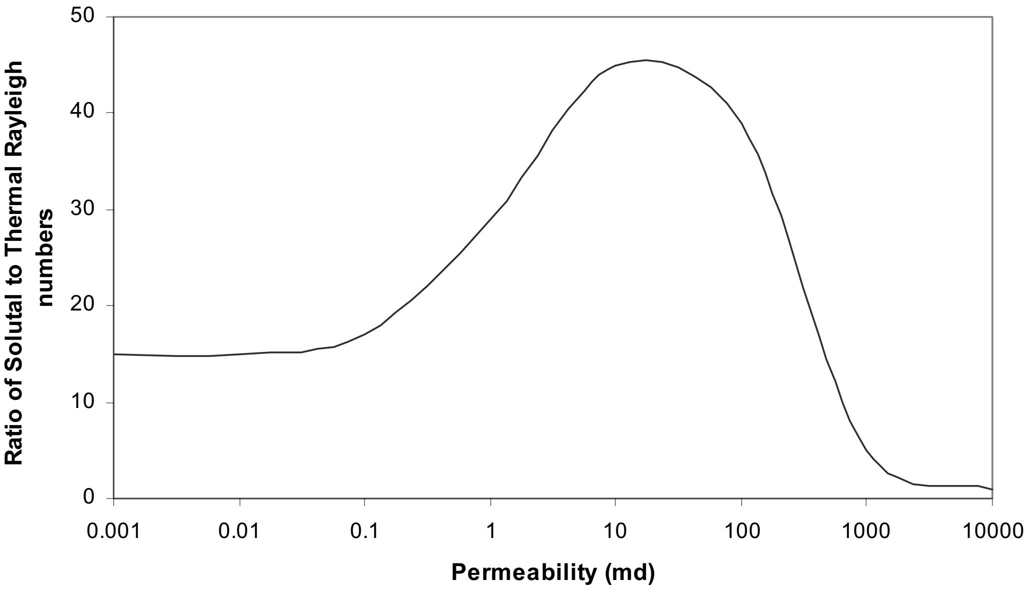

Figure 19 : Variation of the Rayleigh number for THN-C12

Table 1 : Maximum Separation Obtained by Analytical Expression and Numerical Simulation

	Analytical Maximum Separation Ratio [md]	Numerical Maximum Separation Ratio [md]
THN-C12	37.7	25
IBB-C12	53.2	42
THN-IBB	78.3	76

duces a very strong Soret effect in the cavity. As the permeability increases, the fluid is able to move more readily throughout the cavity, hence, the buoyancy-driven convection becomes stronger, and Soret effect becomes less dominant. The analysis reveals a consistent behaviour between the three binary mixtures. It also reveals that the THN-C12 mixture separates the most, while THN-IBB separates the least inside the cavity.

Nomenclature

c	Mole fraction or concentration
C_p	Specific heat at constant pressure
D^M	Molecular diffusion coefficient
D^P	Pressure diffusion coefficient
D^T	Thermal diffusion coefficient
H	Height of a porous cavity
j	Diffusive flux
$\overrightarrow{J}$	Molar flux
k	Thermal conductivity
P	Pressure
∇P	Pressure gradient
q	Separation ratio
S_T	Soret Coefficient
T	Temperature
∇T	Temperature gradient
u	Velocity component in x-direction
v	Velocity in y-direction
$\vec{V}$	Velocity vector in the two dimensional field
∇c	Mole fraction gradient

Greek Letters

κ	Permeability

μ	Dynamic viscosity of fluid mixture
ρ	Mass density of the mixture
ρ_m	Molar density of the mixture
ϕ	Porosity of the porous medium
τ_f	Characteristic time of the convection flow
τ_{th}	Characteristic time of thermodiffusion

Subscripts

o	Reference quantity
e	Effective
f	Fluid mixture
m	Molar quantities

Acknowledgement: The authors acknowledge the full financial support of the Natural Science and Engineering Council (NSERC).

References

Benano-Melly L. B., Caltagirone J. P., Faissat B., Montel F., Costeseque P., (2001): Modeling Soret Coefficient Measurement Experiments in Porous Media Considering Thermal and Solutal Convection, *International Journal of Heat and Mass Transfer*, vol. 44, no. 7, pp. 1285-1297

Chacha M. and Saghir M.Z., (2003): Influence of Thermal Boundary Conditions on the Double-Diffusive Process in a Binary Mixture, *Philosophical Magazine*, vol. 83, no. 17-18, pp. 2109-2129

Costeseque P., Pollak, T., Platten J., Marcoux M., (2004): Simultaneous Evaluation of Soret and Fick Coefficients in a Free and a Packed Vertical Gradient Soret Cell, 6^{th} International Meeting on Thermodiffusion, Varenna, Italy

Firoozabadi A., Ghorayeb K., Shukla K., (2000): Theoretical Model of Thermal Diffusion Factors in Multicomponent Mixtures, *AlChE J.*, vol. 46, pp. 892-900

Firoozabadi A. (1999): *Thermodynamics of Hydrcarbon Reservoirs*, McGraw-Hill, New York

Kempers, L. J. M., (1989): A Thermodynamic Theory of the Soret Effect in a Multicomponent Liquid. *J. Chem. Phys.*, vol. 90, pp. 6541-6548

Jossi, J. A., Stiel, L. I., and Thodos, G., (1962): The viscosity of pure substances in the dense gaseous and liquid phases, *AIChE J.*, vol. 8, pp. 59,.

Lohrenz, J., Bray, B. G., Aime, M., and Clark, C. R., (1964): Calculation of viscosities of reservoir fluids from their compositions, *Journal of Petroleum Technology*, pp. 1171–1176, October.

Lorenz M. and Emery Jr. A. H., (1959): The Packed Thermal Diffusion Column, *Chemical Engineering Science*, vol. 11, no. 1, pp. 16-23

Platten J.K., Bou-Ali M. M. , Costeseque P. , Dutrieux J. F. , Kohler W. , Leppla C. , Wiegand S. , Wittko G. , (2003): Benchmark Values for Soret, Thermal Diffusion and Diffusion Coefficients of Three Binary Organic Liquid Mixtures, *Philosophical Magazine*, vol. 83, pp. 1965 – 1971

Riley M. and Firoozabadi A., (1998): Compositional Variation in Hydrocarbon Reservoirs with Natural Convection and Diffusion, *AlChE J.* , vol. 44, pp. 452-464

Rutherford, W.M. and Roof, J.G., (1959): Thermal Diffusion in Methane n-Butane Mixture in the Critical Region, *J. Phys. Chem.*, vol. 63, pp. 1506-1511

Shukla K., Firoozabadi A., (1998): A New Model of Thermal Diffusion Coefficients in Binary Hydrocarbon Mixtures, *Ind. Engrg. Chem. Res.*, vol. 37, pp. 3331-3342